Probing short-range magnetic order in a geometrically frustrated magnet by spin Seebeck effect

Changjiang Liu,[1,*] Stephen M. Wu,[1,2,*] John E. Pearson,[1] J. Samuel Jiang,[1] N. d'Ambrumenil,[3] and Anand Bhattacharya[1,†]

[1]*Materials Science Division, Argonne National Laboratory, Lemont, Illinois 60439, USA*
[2]*Department of Electrical and Computer Engineering, University of Rochester, Rochester, New York 14627, USA*
[3]*Department of Physics, University of Warwick, Coventry CV4 7AL, UK*

Competing magnetic interactions in geometrically frustrated magnets give rise to new forms of correlated matter, such as spin liquids and spin ices. Characterizing the magnetic structure of these states has been difficult due to the absence of long-range order. Here, we demonstrate that the spin Seebeck effect (SSE) is a sensitive probe of magnetic short-range order (SRO) in geometrically frustrated magnets. In low temperature (2 - 5 K) SSE measurements on a model frustrated magnet $Gd_3Ga_5O_{12}$, we observe modulations in the spin current on top of a smooth background. By comparing to existing neutron diffraction data, we find that these modulations arise from field-induced magnetic ordering that is short-range in nature. The observed SRO is anisotropic with the direction of applied field, which is verified by theoretical calculation.

Pure spin currents carried by magnetic excitations are of fundamental interest and may be used to transmit and store information [1]. One method of generating a pure spin current is through the spin Seebeck effect (SSE), where a thermal gradient drives a current of magnons. Spin currents have been generated in this way using both ferromagnetic (FM) [2] and antiferromagnetic (AFM) [3, 4] magnons. It has been shown that for correlated paramagnetic insulators, a spin current may be generated via the SSE or paramagnetic spin pumping [5, 6]. It is presumed that this is due to short lived magnons (paramagnons) arising as a result of correlations between spins [5, 7–11].

Current understanding of the SSE in magnetic insulators is based on the diffusion of thermally activated magnons [12–15]. Such a mechanism is supported by recent experiments studying the length scale, temperature and magnetic field dependencies of SSE in ferrimagnetic insulator Yttrium Iron Garnet (YIG) [16–18]. The diffusive magnons have finite lifetime and diffusion length. The fact that SSE can be measured in nanometer thickness YIG films and in the picosecond time scale [19] suggests that the SSE is sensitive to magnons in very small volume or with very short lifetimes. These aspects of SSE suggest that it may be used as a sensitive probe of magnetic order in unconventional magnetic materials, such as geometrically frustrated systems.

In this work, we use the SSE to probe the magnetic short-range order (SRO) in a model frustrated magnet gadolinium gallium garnet ($Gd_3Ga_5O_{12}$, GGG). It was shown earlier that the generation of a spin current by SSE does not need magnetic long-range order (LRO) [6, 20]. While this suggests that spin correlations or SRO may play a role, a definitive demonstration of a connection between SRO and the SSE has been missing. Here, we demonstrate for the first time that a specific antiferromagnetic order that is short-range in nature can be detected by the SSE in the absence of LRO.

As is shown in Fig. 1(a), the Gd sites in GGG form a hyperkagome lattice, a three-dimensional kagome lattice consisting of two interpenetrating corner-sharing triangular sublattices [21, 22]. The exchange interaction between nearest-neighbor Gd^{3+} ions are antiferromagnetic. Owing to geometrical frustration on the hyperkagome lattice, GGG hosts an rich phase diagram at low temperatures ($T < 1$ K) [22]. There is no magnetic LRO in GGG down to 25 mK, even though the Curie-Weiss temperature is $\theta_{CW} \sim -2.3$ K [6, 21, 23, 24]. It has been shown that many interesting phases arise within GGG, including spin liquid states [21], protected spin clusters [25] and a hidden multipolar order [26]. In our experiment, we use the SSE to probe magnetic-field-induced SRO in GGG in the temperature regime (2 - 5 K) where effects due to geometric frustration starts to emerge as we approach the magnitude of

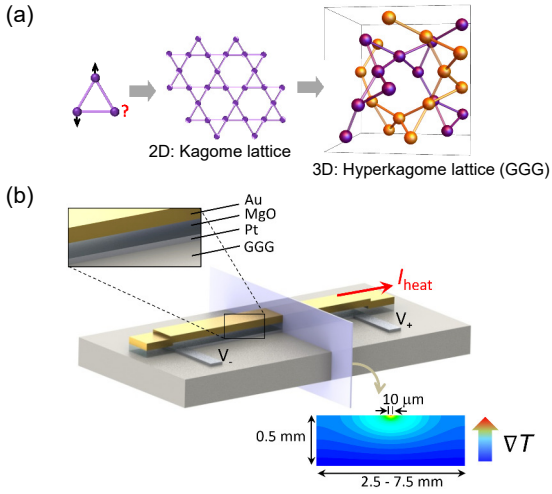

FIG. 1. GGG hyperkagome lattice and schematics of the SSE device. (a) Illustration of geometrical frustration of antiferromagnetically coupled spins on a triangular lattice. Kagome lattice is a realization of such frustration in two dimensional space. When extended to three dimensions, corner-sharing triangles form the hyperkagome lattice. For GGG, the two interpenetrating corner-sharing triangular sublattices are shown in purple and orange, respectively. (b) Device design of an on-chip heated SSE device. Upper left panel shows the vertical structure of the fabricated device. A cross-sectional view of the simulated temperature profile in GGG is shown in the bottom panel.

* These authors contributed equally to this work.
† anand@anl.gov

θ_{CW}.

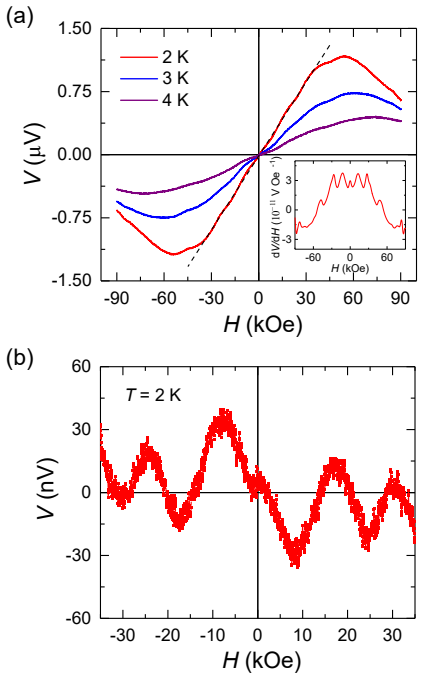

FIG. 2. SSE measurement at low temperatures and modulation in the SSE response. (a) SSE measurement results at temperatures below 5 K. Inset is the derivative of SSE voltage with respect to magnetic field for T = 2 K data. (b) Field-dependent modulation in the SSE response is seen after subtracting a linear background (dashed line in Fig. 2(a)) from the SSE signal in the field range - 35 kOe $< H <$ 35 kOe.

To accomplish this, SSE devices were patterned onto GGG single crystals with polished surface along (111) or (001) (see also Supplemental Material). Platinum (Pt) was used as spin detector material. Local heating was achieved by passing an electric current through a gold heater wire [27], electrically isolated from the spin detector layer by a thin MgO layer. The resulting temperature gradient is perpendicular to the sample plane, which drives spin excitations from the GGG into the Pt detector, where a voltage develops as a result of the inverse spin Hall effect (ISHE). Figure 1(b) depicts the structure of the fabricated SSE device. Using these devices, our measurement results agree with the original SSE experiments on GGG [6] which was carried out at a higher range of temperature ($T > 5$ K). Shown in Fig. 2(a) are the SSE signals measured as a function of magnetic field at different temperatures. The initial rise of SSE response with magnetic field is due to the increase of magnetization of GGG until almost saturation. However, we observe an appreciable downturn in the SSE response at lower temperatures in the high field range, as can be seen in the $T =$ 2 K data. This downturn is presumably caused by the opening of a Zeeman gap in the magnon spectrum, similar to the observation in ferrimagnetic insulator YIG [18, 28, 29]. To confirm this, we performed the SSE measurement down to 200 mK, where the SSE signal is suppressed to zero for $H > 90$ kOe (see Supplementary Fig. 1).

As described above, GGG is not simply a paramagnet. It possesses strong geometric frustration due to antiferromagnetic and dipolar interactions on the hyperkagome lattice. If one considers only the nearest-neighbor antiferromagnetic exchange interaction J, it has been shown that for a hyperkagome lattice a magnetic field with energy scale equal to 6 J or about 17 kOe is required to align those spins in GGG even at $T = 0$ K [30]. Our SSE experiment exhibits this behaviors in that the maximum signal (around saturation) occurs at fields much higher than the value inferred by a Brillouin function for a non-interacting paramagnet at the same low temperature (Supplementary Fig. 2). We note that (and will be discussed later) because of the large dipolar interactions, the magnetic moments in GGG are not fully aligned even at fields beyond 17 kOe.

Upon closer examination, the SSE signals shown in Fig. 2(a) are found not to be smooth functions of magnetic field, but contain considerable field-dependent modulations on top of the S-shaped curve. Inset of Fig. 2(a) shows the derivative of the SSE signal with respect to magnetic field, in which we can clearly see the modulation in the SSE response as a function of field. In Fig. 2(b), the modulation in SSE voltage is plotted directly after subtracting a linear background (indicated by the dashed line in Fig. 2(a)) from the SSE signal in the field range - 35 kOe $< H <$ 35 kOe. When the same experiment is performed on a single crystal YIG sample in the same temperature and magnetic field range, the modulation is absent (Supplementary Fig. 3). We also rule out the possibility of magnetic-field-induced thermal conductivity or heat capacity changes as a possible source for this effect by independently measuring these quantities as a function of applied magnetic field (Supplementary Fig. 4).

In neutron scattering studies on GGG, it has been found that different magnetic orders rise and fall with increasing magnetic field at low temperature (< 400 mK) [22, 31–34]. At higher temperatures ($T \sim 3$ K, as is in our measurement range), short-range correlations are known to persist [21, 35], though little is known about their properties under a magnetic field. The dynamics of thermally excited magnons in this temperature range depends on these short-range correlations, which in turn can influence the SSE signal. It is also known from neutron scattering and bulk magnetometry measurements that the field-induced magnetic orderings in GGG have distinct anisotropies. For instance, the critical field at which the AFM phase emerges [22, 33, 34] depends on the direction of the field relative to the GGG crystal axis, being different for field aligned along [100] versus along [110] crystal axis [22, 36]. Such anisotropy is presumably caused by dipolar interactions among Gd ions [37]. The Gd^{3+} ion in GGG carries a relatively large magnetic moment of 7 μ_B leading to the dipolar interactions with an energy scale comparable to the nearest-neighbor exchange interaction.

To find out whether the modulations in the SSE signal are associated with a field-induced magnetic ordering, we performed the SSE measurements with magnetic field applied along several different GGG crystal axes. The measured SSE signals from the same device are shown in Fig. 3(a), with 0 and 45 degree corresponding to [100] and [110] crystal axes, respectively. Figure 3(b) shows the overall magnitude of the

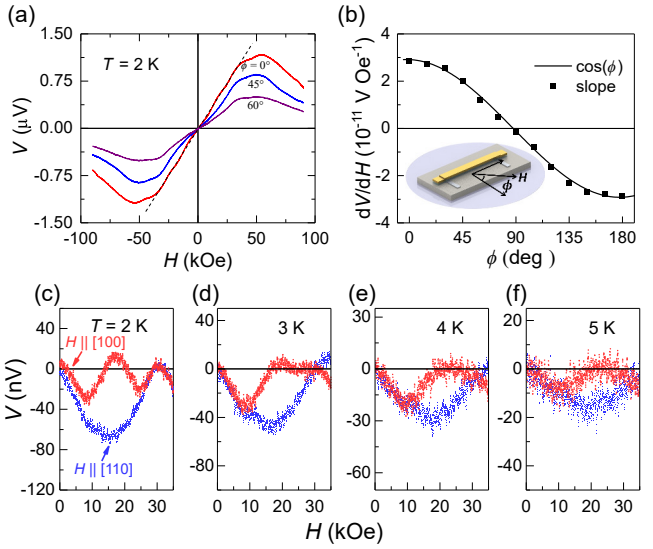

FIG. 3. Anisotropic behavior of the modulation in SSE response. (a) SSE signals measured with magnetic field applied along different directions in the (001) plane, with $\phi = 0°$ being along [100] crystal axis. (b) Magnitude of slope of the linear part of the SSE signal satisfies cosine angular dependence. Inset shows the corresponding measurement geometry. H is the applied in-plane magnetic field. (c) to (f) Modulations in SSE voltage from T = 2 to 5 K. Data in red and blue corresponds to field applied along [100] and [110] directions, respectively. In these measurement, the SSE devices were fabricated on the (001) surface of GGG signal crystals.

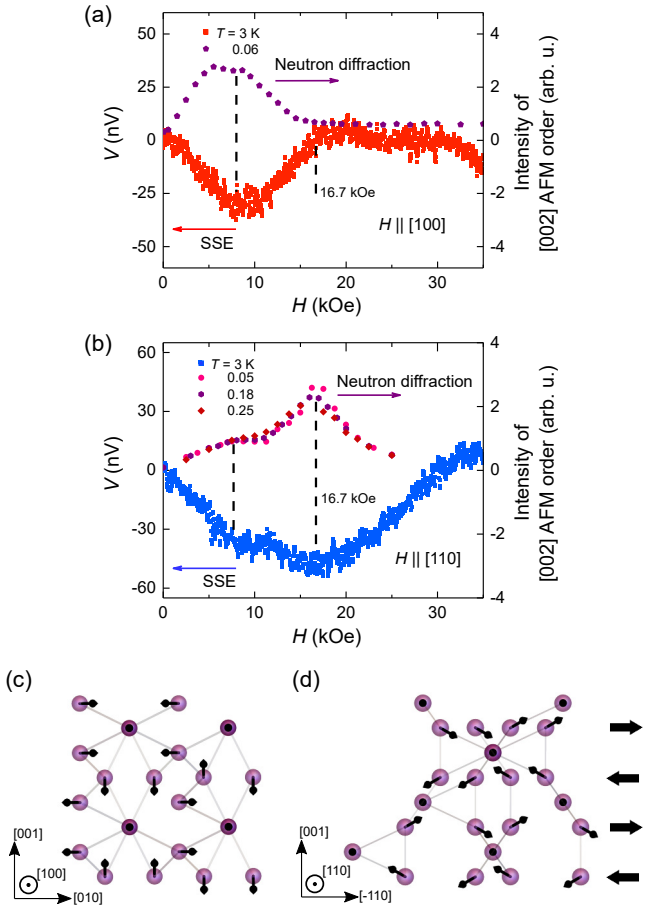

FIG. 4. Comparison between the SSE response and the intensity of [002] AFM order, and theoretical calculation of spin configurations. (a) and (b) Magnetic field dependencies of the modulation in SSE signal and the intensity of [002] AFM order measured by neutron diffraction with corresponding field applied along [100] and [110] crystal axes, respectively. Vertical dashed lines in both (a) and (b) indicate the same peak positions in the SSE data and neutron diffraction results. (c) and (d) Calculated spin configurations in one GGG primitive cell at an applied field $H = 17$ kOe aligned along [100] and [110] crystal axes, respectively. The magnetic field points out of the page, and the spin orientation of Gd^{3+} ions is represented by an small arrow at each Gd site. Notice that most spins are canted away from the applied field. In (c) the net spin components in horizontal direction are zero, while the total horizontal components in (d), indicated by large arrows on the right, form an alternating AFM pattern.

SSE signal, represented by the slope of the linear background at low fields, as a function of the in-plane angle of the magnetic field. The data is fit well by a cosine function which is expected from the geometry of the ISHE, and implies that the linear background is isotropic and independent of the direction of magnetic field. In Fig. 3(c) - (f), the modulations in the SSE signal are presented for temperatures from 2 to 5 K. In these plots, red and blue data correspond to field applied along [100] and [110] GGG crystal axes, respectively. For clarity, only data for the positive field range is plotted. The magnitude of these modulations becomes smaller as temperature increases. At each temperature, the magnetic-field dependences of the modulation are clearly different between the two field orientations. For instance, in Fig. 3(c), when the field is applied along [100] direction, the modulation initially decreases with magnetic field and reaches a minimum at $H \sim 8$ kOe, while the minimum for field parallel to [110] direction occurs at $H \sim 17$ kOe. This same trend is observed at higher temperatures up to 5 K. At $T = 2$ K, however, there is a second minimum at higher field $H \sim 24.5$ kOe for field along [100] direction, which is suppressed at $T > 3$ K suggesting that this may have a different origin than the modulations at lower fields.

Magnetic ordering in GGG has been extensively studied over the last two decades, and a summary of these results is presented in the Supplementary Material. Upon application of a magnetic field at low temperatures there are FM, AFM and incommensurate AFM LRO that emerge in GGG. Most of the AFM orderings, including all incommensurate ones, have a strong temperature dependence, and they are suppressed at $T > 400$ mK [22]. However, of particular interest is the [002] AFM order, whose intensity is observable up to 900 mK [33, 34], above which there is no published experimental data, though LRO is completely suppressed by 1.3 K (see Supplementary Fig. 5). Shown in Fig. 4(a) (reproduced from Ref. [33]) are the integrated intensity of the [002] AFM peak as a function of magnetic field with the field applied along [100] direction. We see that the maximum position of the neutron scattering data matches the field, indicated by the vertical dashed line, where the modulation in SSE voltage shows a

minimum. Crucially, for field applied along [110] direction, the [002] AFM order reaches its maximum at $H \sim 16.7$ kOe as shown in Fig. 4(b) (reproduced from Ref. [34]) which is also in good agreement with corresponding SSE measurement results. Additionally, a small inflection in the SSE data for $H \parallel [110]$ can be seen at $H \sim 7.7$ kOe, that is also present in the neutron diffraction result. Over the entire temperature range available, the peak positions in neutron scattering data and the minima of our SSE modulations show little temperature dependence. Any remaining discrepancies may be due to non-uniform crystal shape in the neutron diffraction experiments where the demagnetization field is not considered. These comparisons provide strong evidence that the modulation observed in the SSE measurement is associated with the [002] AFM order. The temperatures used in the SSE measurement are much higher than that for the disappearance of LRO peaks as measured in neutron scattering experiments [22] (see also Supplementary Fig. 5) implying that this magnetic order is short range in character.

In order to understand the anisotropic behaviors observed in the SSE experiment, we have computed the spin order in GGG in the presence of a magnetic field using a Hamiltonian including exchange (J) and dipolar (D) interactions (see also Supplementary Note):

$$H = \sum_{j\alpha,l\beta} J_{j\alpha,l\beta}\mathbf{S}_{j\alpha}\cdot\mathbf{S}_{l\beta} - g\mu_B H\sum_{j\alpha} S^z_{j\alpha} + D\sum_{j\alpha,l\beta}\left(\frac{\mathbf{S}_{j\alpha}\cdot\mathbf{S}_{l\beta} - 3(\mathbf{S}_{j\alpha}\cdot\hat{r}_{j\alpha l\beta})(\mathbf{S}_{l\beta}\cdot\hat{r}_{j\alpha l\beta})}{r^3_{j\alpha l\beta}}\right), \quad (1)$$

where vectors $\mathbf{S}$ represent the spins at each Gd site with indices j, l identifying the unit cell, and α, β indicating the twelve Gd ions in the primitive cell, respectively. The second term in the Hamiltonian comes from the applied magnetic field H, with g and μ_B being the g-factor of Gd ions and Bohr magneton, respectively. The vectors $\hat{r}$ denote unit vectors along the direction from site $j\alpha$ to site $l\beta$. An example of the calculated spin configurations are shown in Fig. 4(c) and (d), with $H = 17$ kOe applied along [100] and [110] GGG crystal axes, respectively. In each graph, the perspective is chosen such that the magnetic field points out of the page. In both cases, spins at most of the Gd sites are canted away (showing transverse components) from the applied field as a result of the exchange and dipolar interactions. At $H \sim 17$ kOe, the modulation in SSE signal is almost zero for field along [100] (Fig. 4(a)), while its magnitude becomes largest for field along [110] (Fig. 4(b)),. Correspondingly, our calculation of the spin configuration shows that the magnetic ordering is different between the two cases. For field along [110], we find that the canting of spins leads to a net magnetization within each layer (Fig. 4(d)), with AFM ordering between layers at the [002] wavevector, as is also observed in neutron scattering measurement. In contrast, when the same field is applied along [100] (Fig. 4(c)), no AFM order develops.

In general, the SSE is associated with two effects, the magnetization carried by thermally excited magnons and their diffusivity. According to our calculation, the total magnetization of GGG at $H = 17$ kOe, taking into account the canting of spins, is very similar for the two field directions. This suggests that the large isotropic 'background' SSE signal may originate from excitations derived from the total magnetization. In contrast, the magnetic order due to the canting of spins is different for the two field directions. This suggests that the modulations in the SSE signal, which decreases as AFM order increases, could be due to a decrease in the number of magnons excited since AFM ordering may lead to a gap in the spin-wave excitation spectrum [38]. The decrease in SSE could also be due to changes in the spin-wave dispersion with the onset of AFM order that lower the diffusivity of magnons.

In conclusion, we have demonstrated that the spin Seebeck effect, in addition to serving as a generator of spin current for spintronics applications, can also be used as a more general technique to probe magnetic order in a larger class of condensed matter systems, such as geometrically frustrated magnets studied in this work. For gadolinium gallium garnet, our SSE measurements have revealed a field-induced, anisotropic short-range order that persists to high temperatures (up to 5 K), which was not known previously. This new approach, where we use SSE to probe magnetic structures in the absence of long-range order, opens the door to exploring frustrated quantum magnetic systems, particularly for samples with limited volume such as exfoliated materials and thin films. This would allow us to probe collective excitations that are *only* short-ranged in nature, and thus entirely hidden to the community, and serve as a guide for large-scale neutron or x-ray scattering experiments.

ACKNOWLEDGMENTS

We acknowledge very valuable discussions with Oleg Petrenko and thank him for sharing neutron data on GGG. All work at Argonne was supported by the U.S. Department of Energy, Office of Science, Basic Energy Sciences, Materials Sciences and Engineering Division. The use of facilities at the Center for Nanoscale Materials, an Office of Science user facility, was supported by the U.S. Department of Energy, Basic Energy Sciences under contract No. DEAC02-06CH11357.

[1] G. E. W. Bauer, E. Saitoh, and B. J. van Wees, Nat. Mater. **11**, 391 (2012).

[2] K.-i. Uchida, H. Adachi, T. Ota, H. Nakayama, S. Maekawa, and E. Saitoh, Appl. Phys. Lett. **97**, 172505 (2010).

[3] S. M. Wu, W. Zhang, A. KC, P. Borisov, J. E. Pearson, J. S. Jiang, D. Lederman, A. Hoffmann, and A. Bhattacharya, Phys. Rev. Lett. **116**, 097204 (2016).

[4] S. Seki, T. Ideue, M. Kubota, Y. Kozuka, R. Takagi, M. Nakamura, Y. Kaneko, M. Kawasaki, and Y. Tokura, Phys. Rev. Lett. **115**, 266601 (2015).

[5] Y. Shiomi and E. Saitoh, Phys. Rev. Lett. **113**, 266602 (2014).
[6] S. M. Wu, J. E. Pearson, and A. Bhattacharya, Phys. Rev. Lett. **114**, 186602 (2015).
[7] P. A. Fleury, Phys. Rev. **180**, 591 (1969).
[8] F. Mila, D. Poilblanc, and C. Bruder, Phys. Rev. B **43**, 7891 (1991).
[9] R. Doubble, S. M. Hayden, P. Dai, H. A. Mook, J. R. Thompson, and C. D. Frost, Phys. Rev. Lett. **105**, 027207 (2010).
[10] S. Okamoto, Phys. Rev. B **93**, 064421 (2016).
[11] H. J. Qin, K. Zakeri, A. Ernst, and J. Kirschner, Phys. Rev. Lett. **118**, 127203 (2017).
[12] J. Xiao, G. E. W. Bauer, K.-c. Uchida, E. Saitoh, and S. Maekawa, Phys. Rev. B **81**, 214418 (2010).
[13] H. Adachi, K. ichi Uchida, E. Saitoh, and S. Maekawa, Rep. Prog. Phys. **76**, 036501 (2013).
[14] S. Rezende, R. RodrÃguez-SuÃ¡rez, R. Cunha, J. L. Ortiz, and A. Azevedo, J. Magn. Magn. Mater. **400**, 171 (2016).
[15] S. M. Rezende, R. L. Rodríguez-Suárez, and A. Azevedo, Phys. Rev. B **93**, 014425 (2016).
[16] A. Kehlberger, U. Ritzmann, D. Hinzke, E.-J. Guo, J. Cramer, G. Jakob, M. C. Onbasli, D. H. Kim, C. A. Ross, M. B. Jungfleisch, B. Hillebrands, U. Nowak, and M. Kläui, Phys. Rev. Lett. **115**, 096602 (2015).
[17] K.-i. Uchida, T. Kikkawa, A. Miura, J. Shiomi, and E. Saitoh, Phys. Rev. X **4**, 041023 (2014).
[18] U. Ritzmann, D. Hinzke, A. Kehlberger, E.-J. Guo, M. Kläui, and U. Nowak, Phys. Rev. B **92**, 174411 (2015).
[19] J. Kimling, G.-M. Choi, J. T. Brangham, T. Matalla-Wagner, T. Huebner, T. Kuschel, F. Yang, and D. G. Cahill, Phys. Rev. Lett. **118**, 057201 (2017).
[20] D. Hirobe, M. Sato, T. Kawamata, Y. Shiomi, K.-i. Uchida, R. Iguchi, Y. Koike, S. Maekawa, and E. Saitoh, Nat. Phys. **13**, 30 (2017).
[21] O. A. Petrenko, C. Ritter, M. Yethiraj, and D. McK Paul, Phys. Rev. Lett. **80**, 4570 (1998).
[22] P. P. Deen, O. Florea, E. Lhotel, and H. Jacobsen, Phys. Rev. B **91**, 014419 (2015).
[23] W. I. Kinney and W. P. Wolf, J. Appl. Phys. **50**, 2115 (1979).
[24] S. R. Dunsiger, J. S. Gardner, J. A. Chakhalian, A. L. Cornelius, M. Jaime, R. F. Kiefl, R. Movshovich, W. A. MacFarlane, R. I. Miller, J. E. Sonier, and B. D. Gaulin, Phys. Rev. Lett. **85**, 3504 (2000).
[25] S. Ghosh, T. F. Rosenbaum, and G. Aeppli, Phys. Rev. Lett. **101**, 157205 (2008).
[26] J. A. M. Paddison, H. Jacobsen, O. A. Petrenko, M. T. Fernández-Díaz, P. P. Deen, and A. L. Goodwin, Science **350**, 179 (2015).
[27] S. M. Wu, F. Y. Fradin, J. Hoffman, A. Hoffmann, and A. Bhattacharya, J. Appl. Phys. **117**, 17C509 (2015).
[28] T. Kikkawa, K.-i. Uchida, S. Daimon, Z. Qiu, Y. Shiomi, and E. Saitoh, Phys. Rev. B **92**, 064413 (2015).
[29] E.-J. Guo, J. Cramer, A. Kehlberger, C. A. Ferguson, D. A. MacLaren, G. Jakob, and M. Kläui, Phys. Rev. X **6**, 031012 (2016).
[30] M. E. Zhitomirsky, A. Honecker, and O. A. Petrenko, Phys. Rev. Lett. **85**, 3269 (2000).
[31] P. Schiffer, A. P. Ramirez, D. A. Huse, and A. J. Valentino, Phys. Rev. Lett. **73**, 2500 (1994).
[32] O. Petrenko, D. Paul, C. Ritter, T. Zeiske, and M. Yethiraj, Physica B **266**, 41 (1999).
[33] O. Petrenko, G. Balakrishnan, D. McK Paul, M. Yethiraj, and J. Klenke, Appl. Phys. A **74**, s760 (2002).
[34] O. A. Petrenko, G. Balakrishnan, D. M. Paul, M. Yethiraj, G. J. McIntyre, and A. S. Wills, J. Phys. Conf. Ser. **145**, 012026 (2009).
[35] O. A. Petrenko and D. McK. Paul, Phys. Rev. B **63**, 024409 (2000).
[36] A. Rousseau, J.-M. Parent, and J. A. Quilliam, Phys. Rev. B **96**, 060411 (2017).
[37] N. d'Ambrumenil, O. A. Petrenko, H. Mutka, and P. P. Deen, Phys. Rev. Lett. **114**, 227203 (2015).
[38] J. A. Quilliam, K. A. Ross, A. G. Del Maestro, M. J. P. Gingras, L. R. Corruccini, and J. B. Kycia, Phys. Rev. Lett. **99**, 097201 (2007).